The Astrophysical Journal Letters, 984:L40 (5pp), 2025 May 10 https://doi.org/10.3847/2041-8213/adcc30

Cosmological Parameter Estimate from Persistent Radio Sources of Fast Radio Bursts

Zi-Liang Zhang (张子良)[1,2] and Bing Zhang (张冰)[1,2]
[1] Nevada Center for Astrophysics, University of Nevada, Las Vegas, NV 89154, USA; ziliang.zhang@unlv.edu, bing.zhang@unlv.edu
[2] Department of Physics and Astronomy, University of Nevada, Las Vegas, NV 89154, USA
Received 2025 March 19; revised 2025 April 7; accepted 2025 April 14; published 2025 May 2

Abstract

We introduce a novel method to constrain the Hubble constant (H_0) by combining fast radio bursts (FRBs) and their persistent radio sources (PRSs) through the observationally validated Yang relation, $L_\nu \propto |\mathrm{RM}|$, which links PRS luminosity to the rotation measure of the associated FRB. Using a mock sample of PRSs, we demonstrate that the Yang relation can help to unravel the degeneracies among H_0, baryon density parameter Ω_b, and baryon fraction in the intergalactic medium $f_{\rm IGM}$ in the traditional approach of using dispersion measure only to perform cosmological analyses. Our method employs a two-stage Markov Chain Monte Carlo analysis to constrain H_0. Using the available data of six observed PRS systems, we obtain a preliminary constraint of $H_0 = 75 \pm 30\,\mathrm{km\,s^{-1}\,Mpc^{-1}}$. We briefly discuss possible refinements of the method by reducing residual degeneracies and systematic uncertainties using future data and physical modeling. Our results indicate that the Yang relation can potentially become a new probe for performing FRB cosmology.

Unified Astronomy Thesaurus concepts: Radio bursts (1339); Radio sources (1358); Radio continuum emission (1340); Hubble constant (758); Cosmological parameters (339)

1. Introduction

Fast radio bursts (FRBs) are millisecond-duration radio transients of extragalactic origin (D. R. Lorimer et al. 2007; D. Thornton et al. 2013; J. M. Cordes & S. Chatterjee 2019; E. Petroff et al. 2022; B. Zhang 2023) with the potential of serving as a new type of cosmological probe (S. Bhandari & C. Flynn 2021; M. Glowacki & K.-G. Lee 2024; Q. Wu & F.-Y. Wang 2024).

The dispersion measure (DM), defined as the column density of free electrons along the line of sight, serves as a key diagnostic by encoding information about the electron distribution in intervening environments. Consequently, FRB-based studies have been employed to trace missing baryons in the intergalactic medium (IGM; e.g., W. Deng & B. Zhang 2014; J. P. Macquart et al. 2020; Z. Li et al. 2020b), characterize inhomogeneities in the IGM (e.g., M. McQuinn 2014), map large-scale fluctuations (e.g., J. P. Macquart et al. 2020; Q. Wu et al. 2022), constrain the Hubble constant (H_0; e.g., Q. Wu et al. 2022), reconstruct reionization history (e.g., W. Deng & B. Zhang 2014; Z. Zheng et al. 2014; M. Caleb et al. 2019; P. Beniamini et al. 2021), and probe dark energy (e.g., H. Gao et al. 2014; B. Zhou et al. 2014; Y.-Y. Wang et al. 2025).

Currently, there is an inconsistency in measuring the Hubble constant H_0 using different methods. Measurements of H_0 from late-Universe distance-ladder methods (e.g., $H_0 = 73.04 \pm 1.04\,\mathrm{km\,s^{-1}\,Mpc^{-1}}$, A. G. Riess et al. 2022) conflict with those derived from early-Universe cosmic microwave background observations (e.g., $H_0 = 67.4 \pm 0.5\,\mathrm{km\,s^{-1}\,Mpc^{-1}}$, Planck Collaboration et al. 2020). Independent measurements of H_0 would be helpful to resolve the tension, and FRBs offer such an opportunity.

However, measurements of H_0 using the intergalactic DM component, $\mathrm{DM_{IGM}}$, are limited by inherent parameter correlations. As shown in Equation (5), $\mathrm{DM_{IGM}}$ introduces degeneracies among H_0, the baryon density parameter Ω_b, and the baryon fraction in the IGM, $f_{\rm IGM}$.[3] Further uncertainties arise from intrinsic variations in $\mathrm{DM_{IGM}}$ and its degeneracy with host galaxy DM contributions.

Persistent radio sources (PRSs) are steady radio emitters, typically observed at gigahertz frequencies with luminosities of around $10^{29}\,\mathrm{erg\,s^{-1}\,Hz^{-1}}$ and confined to regions smaller than a parsec. These sources are associated with a subset of repeating FRBs. The first confirmed PRS was discovered in 2017, linked to FRB 20121102A (S. Chatterjee et al. 2017). Observations of its size, luminosity, and spectral properties rule out the possibility of a coincidental association with nearby star formation activity (C. G. Bassa et al. 2017; S. Chatterjee et al. 2017; M. Kokubo et al. 2017; S. P. Tendulkar et al. 2017), indicating that PRSs are associated with the FRB's central engine, likely through synchrotron emission.

Before the discovery of PRSs, theoretical studies had predicted steady synchrotron radiation from FRB central engines (K. Murase et al. 2016; Y.-P. Yang et al. 2016). Following the detection of the PRS linked to FRB 20121102A, multiple models emerged to explain PRS origins (Z. G. Dai et al. 2017; B. D. Metzger et al. 2017; B. Margalit & B. D. Metzger 2018; B. Margalit et al. 2018, 2019; Q.-C. Li et al. 2020a; Z. Y. Zhao & F. Y. Wang 2021; N. Sridhar & B. D. Metzger 2022). In particular, Y.-P. Yang et al. (2020) proposed a generic model of synchrotron-emitting nebula and derived a simple linear relation between PRS luminosity and FRB rotation measure (RM). This "Yang relation" (Equation (1)) governed by the magneto-ionic environment of FRBs naturally explains why FRB 20121102A (with the highest known RM) hosts a bright PRS, while FRBs with lower RM values typically lack such counterparts. Recent detections of three additional PRSs (C. H. Niu et al. 2022; Y. Bhusare et al. 2024; G. Bruni et al. 2024, 2025; X. Zhang et al. 2025) and two candidate systems (A. L. Ibik et al. 2024) further

[3] The parameter $f_{\rm IGM}$ here denotes the fraction of baryons in the diffuse medium between the FRB host and Milky Way, which strictly also includes contributions from the intervening galaxy halos along the line of sight, so in the literature it is also called $f_{\rm diff}$ (J. X. Prochaska & Y. Zheng 2019; Z. J. Zhang et al. 2025).

validate the Yang relation, with no significant outliers observed to date.

The Yang relation enables intrinsic luminosity estimation through RM observations, establishing PRSs as viable cosmological probes. We apply this relation to constrain H_0. Given that the number of confirmed PRS systems remains limited, our analysis focuses on a mock PRS sample generated through Monte Carlo simulations, which illustrates the potential of applying the Yang relation as a standard candle while also providing preliminary constraints on H_0 by observed PRSs.

The remainder of this Letter is organized as follows: Section 2 provides a brief description of the Yang relation and the setup of the PRS population for Monte Carlo simulations. Section 3 outlines the analysis procedures and results. Finally, Section 4 summarizes our findings and discusses possible improvements to the methodology.

2. Method

2.1. Luminosity, Rotation Measure, and Dispersion Measure

The luminosity of PRSs is related to the RM via the relation presented by Y.-P. Yang et al. (2020, 2022) and G. Bruni et al. (2024):

$$L_\nu = \frac{64\pi^3}{27} m_e c^2 \zeta_e \gamma_{\rm th}^2 R^2 |{\rm RM_{src}}|, \tag{1}$$

where ${\rm RM_{src}} = (1+z)^2 {\rm RM_{obs}}$.[4] Here, R denotes the emission region radius, ζ_e denotes the ratio between the relativistic and nonrelativistic electron numbers, and $\gamma_{\rm th}$ denotes the minimum Lorentz factor of nonthermal electrons. In this picture, the FRB central engine is at the center of a synchrotron nebula. The relativistic electrons primarily dominate the synchrotron luminosity, while thermal electrons dominate the RM, because RM$\propto (\gamma^2 m_e)^{-1}$ (E. Quataert & A. Gruzinov 2000; Y.-P. Yang et al. 2022). The characteristic Lorentz factor $\gamma_{\rm th}$ marks the transition between these two populations, representing the typical energy that separates the thermal electrons responsible for the RM from the more energetic electrons that drive the observed emission.

Combining the luminosity relation with standard formula for flux density $L_\nu = 4\pi F_\nu \frac{1}{1+z}\left[\frac{c(1+z)}{H_0}\int_0^z \frac{1}{E(z')}dz'\right]^2$ leads to

$$|{\rm RM_{obs}}| = \frac{27}{16\pi^2 m_e}\frac{1}{\zeta_e \gamma_{\rm th}^2 R^2 H_0^2} \times \frac{F_\nu}{1+z}\left(\int_0^z \frac{1}{E(z')}dz'\right)^2, \tag{2}$$

where $E(z) = H(z)/H_0$ is the Hubble parameter normalized by the Hubble constant. We focus on the ΛCDM framework with $E(z) = \sqrt{\Omega_m (1+z)^3 + 1 - \Omega_m}$ in this work. Notice the degeneracy between the product $\zeta_e \gamma_{\rm th}^2 R^2$ and the Hubble constant H_0. Recent observational findings suggest that the product $\zeta_e \gamma_{\rm th}^2 (R/0.01\ \ {\rm pc})^2$ is approximately 1 (G. Bruni et al. 2025). However, simply calculating the luminosity involves H_0, creating a circular argument. To avoid this issue and break the degeneracy, we need an independent constraint for $\zeta_e \gamma_{\rm th}^2 R^2$. One natural method for obtaining this constraint is by using DM.

The total observed DM is the sum of contributions from multiple astrophysical components (e.g., D. Thornton et al. 2013; W. Deng & B. Zhang 2014):

$${\rm DM_{obs}} = {\rm DM_{MW}} + {\rm DM_{halo}} + {\rm DM_{IGM}} + \frac{{\rm DM_{host}} + {\rm DM_{src}}}{1+z}, \tag{3}$$

where $\rm DM_{MW}$, $\rm DM_{halo}$, $\rm DM_{IGM}$, $\rm DM_{host}$, and $\rm DM_{src}$ denote the contributions from the Milky Way's interstellar medium, Galactic halo, IGM, host galaxy's interstellar medium, and the FRB's local environment, respectively. The Galactic contribution, $\rm DM_{MW}$, is estimated using the YWM16 (J. M. Yao et al. 2017) or NE2001 (J. M. Cordes & T. J. W. Lazio 2002) electron density models. For the present analysis, we focus mainly on the extragalactic contributions:

$$\begin{aligned}{\rm DM_{ex}} &= {\rm DM_{obs}} - {\rm DM_{MW}} - {\rm DM_{halo}} \\ &= {\rm DM_{IGM}} + \frac{{\rm DM_{host}} + {\rm DM_{src}}}{1+z}.\end{aligned} \tag{4}$$

The average IGM DM is expressed as (e.g., W. Deng & B. Zhang 2014; J. P. Macquart et al. 2020)

$${\rm DM_{IGM}}(z) = \frac{3cf_{\rm IGM}\Omega_b H_0^2}{8\pi G m_p H_0}\int_0^z \frac{\chi(1+z')}{E(z')}{\rm d}z', \tag{5}$$

where $\chi = 7/8$ denotes the electron fraction from ionized hydrogen and helium. Here we adopt $f_{\rm IGM} \approx 0.83$ following (M. Fukugita et al. 1998) but again note the small difference between $f_{\rm IGM}$ and $f_{\rm diff}$ (up to 5%, e.g., from the simulation of Z. J. Zhang et al. 2025). The degeneracy between $\Omega_b h^2$ and H_0 is alleviated by adopting $\Omega_b h^2 \approx 0.0223$ (Q. Wu et al. 2022), as derived from quasar absorption observations (R. J. Cooke et al. 2018).

Previous literature frequently adopts ${\rm DM_{host}} + {\rm DM_{src}} \sim 100\ {\rm pc\ cm^{-3}}$ to extract $\rm DM_{IGM}$ for cosmological studies (e.g., Z. Li et al. 2020b; B. Zhang 2023). This simple treatment, however, may not apply to our analysis, which focuses on the PRS-associated FRBs that typically have larger values of ${\rm DM_{host}} + {\rm DM_{src}}$ (e.g., Y.-P. Yang et al. 2017; C. H. Niu et al. 2022; V. Ravi et al. 2022; X.-L. Chen et al. 2025). This is consistent with the implication from their magneto-ionic environments (D. Michilli et al. 2018; H. Xu et al. 2022; R. Anna-Thomas et al. 2023). Given these uncertainties, we treat ${\rm DM_{host}} + {\rm DM_{src}}$ as a free parameter in our analysis, avoiding biased assumptions.

By eliminating H_0 from Equation (5) using Equation (2) and substituting the result into Equation (4), we derive

$${\rm DM_{ex}} = \left(\frac{m_e c^2 f_{\rm IGM}^2 \chi^2 \Omega_b^2 H_0^4}{12 G^2 m_p^2} \times \frac{\zeta_e \gamma_c^2 R^2 (1+z)|{\rm RM_{obs}}|}{}F_\nu\right)^{1/2} \frac{\int_0^z \frac{1+z'}{E(z')}dz'}{\int_0^z \frac{1}{E(z')}dz'} + \frac{{\rm DM_{host}} + {\rm DM_{src}}}{1+z}. \tag{6}$$

We can constrain $\zeta_e \gamma_{\rm th}^2 R^2$ by fitting $\rm DM_{ex}$ with z, F_ν and $RM_{\rm obs}$.

[4] In principle, the observed RM consists of five components like DM in Equation (3). However, due to the weak and random IGM magnetic field, RM from IGM could be ignored. From observation and the simulated RM map of the Milky Way (S. Reissl et al. 2023), the Milky Way RM can also be neglected, even for low galactic latitude FRBs (FRB 20121102A and FRB 20201124A). This issue should be carefully considered in the future when there are more PRS sources.

The uncertainty of $\mathrm{DM_{ex}}$ is quantified as

$$\sigma_{\mathrm{DM_{ex}}} = \sqrt{\sigma_{\mathrm{MW}}^2 + \sigma_{\mathrm{IGM}}(z)^2 + \sigma_{\mathrm{host+src}}^2}, \quad (7)$$

where $\sigma_{\mathrm{MW}} \approx 30\,\mathrm{pc\,cm^{-3}}$ (from the uncertainty of Galactic electron number density model R. N. Manchester et al. 2005) represents the combined uncertainty from $\mathrm{DM_{MW}}$ and $\mathrm{DM_{halo}}$. The term $\sigma_{\mathrm{IGM}}(z)$ denotes the uncertainty of $\mathrm{DM_{IGM}}$. Following Z. Li et al. (2020b), we derive it by fitting numerical simulations from M. McQuinn (2014). We adopt $\sigma_{\mathrm{host+src}} \approx 100\,\mathrm{pc\,cm^{-3}}$, a conservative estimate that exceeds the typical values of the FRB observations (J. S. Chittidi et al. 2021; L. Bernales-Cortes et al. 2025) and simulations (G. Q. Zhang et al. 2020; J.-F. Mo et al. 2023; T. O. Kovacs et al. 2024; M. E. Orr et al. 2024; A. Theis et al. 2024; X. Zhang et al. 2025) to account for additional environmental uncertainties in PRS systems.

2.2. PRS Redshift and Luminosity Distribution

To validate our methodology, we employ Monte Carlo simulations to generate mock PRS samples and reconstruct H_0. This process requires two population functions: a redshift distribution and a luminosity function for PRSs. Although our analysis is not critically dependent on the true forms of these functions, we adopt observationally motivated models to replicate observed trends and provide preliminary predictions for the PRS population.

The origin of FRBs remains under debate. Two possibilities have been suggested and gained observational support. One hypothesis proposes that they arise from core-collapse supernovae, implying that the redshift distribution follows the cosmic star formation history (e.g., C. W. James et al. 2022a, 2022b; K. Shin et al. 2023; Y. Wang & J. van Leeuwen 2024). Alternatively, there are suggestions that at least a fraction of FRBs have an origin with a delay with respect to star formation history (e.g., R. C. Zhang & B. Zhang 2022; Z.-L. Zhang et al. 2023; O. Gupta et al. 2025).

For the specific sample we are studying, current data strongly associate PRS-linked FRBs with young stellar environments, since every confirmed PRS-FRB system has been observed in a dwarf galaxy or an actively star-forming galaxy (S. P. Tendulkar et al. 2017; Y. Li et al. 2019; Y. Li & B. Zhang 2020; L. Piro et al. 2021; C. H. Niu et al. 2022; V. Ravi et al. 2022; X.-L. Chen et al. 2025). Even the two candidate PRSs appear to be hosted by star-forming galaxies (A. L. Ibik et al. 2024). Consequently, we adopt the cosmic star formation history as the basis for the redshift distribution $\Psi(z)$ of PRS-associated FRBs, using Equation (15) of P. Madau & M. Dickinson (2014; shown as the gray solid line in the upper panel of Figure 1).[5] In addition, we assume a power-law luminosity function of the form $\Phi(L_\nu) \propto L_\nu^{-1.3}$ (also illustrated by the gray solid line in the upper panel of Figure 1) for PRSs, which closely reproduces the observed luminosity distribution.

3. Result

We perform Markov Chain Monte Carlo (MCMC) analyses to estimate H_0, using about 50 mock PRS detections and observational data. The observational sample includes four confirmed PRSs (S. Chatterjee et al. 2017; C. H. Niu et al. 2022; Y. Bhusare et al. 2024; G. Bruni et al. 2024, 2025; X. Zhang et al. 2025) and two candidate PRSs (A. L. Ibik et al. 2024).

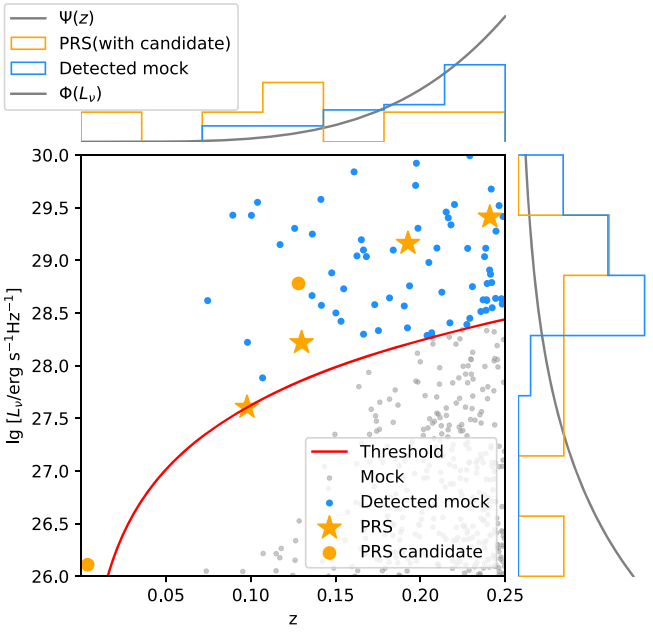

Figure 1. Observed and simulated PRS population. Main panel: luminosity–redshift distribution for mock (gray/blue) and observed PRSs (orange). The red curve indicates the detection threshold. Upper/right panels: intrinsic redshift distribution $\Psi(z)$ and luminosity function $\Phi(L_\nu)$ (gray), compared to detected mock PRSs (blue).

The analysis proceeds as follows:

1. *Mock Sample Generation*. Mock PRS sources are generated by drawing (z, L_ν) pairs from the redshift distribution $\Psi(z)$ and luminosity function $\Phi(L_\nu)$, shown as gray and blue points in Figure 1. The specific flux F_ν for each source is calculated, and sources exceeding the detection threshold of 0.02 mJy (the minimum sensitivity for detected PRSs) are classified as detectable (blue points in Figure 1).
2. *Parameter Initialization*. For the detectable mock PRSs, $\mathrm{DM_{IGM}}$ is computed using Equation (5) with $\Omega_m = 0.34$ and $H_0 = 73.04\,\mathrm{km\,s^{-1}\,Mpc^{-1}}$ (A. G. Riess et al. 2022), since FRBs are local Universe phenomena. The parameter $\zeta_e \gamma_{\mathrm{th}}^2 (R/0.01\quad \mathrm{pc})^2$ is assigned values from a log-normal distribution ($\mu = -0.333$, $\sigma = 0.6$; e.g., G. Bruni et al. 2025), and $|\mathrm{RM_{src}}|$ is calculated using Equation (1). The combined $\mathrm{DM_{host}} + \mathrm{DM_{src}}$ is drawn from a log-normal distribution ($\mu = 6$, $\sigma = 0.6$). Finally, $\mathrm{DM_{ex}}$ values for mock PRS are derived using Equation (6).
3. *First-stage MCMC*. Equation (6) is fitted to each sample set, with the uncertainty shown in Equation (7). Priors include a Gaussian distribution for $\Omega_m = 0.34 \pm 0.03$ to include both early- and late-Universe results (Planck Collaboration et al. 2020; A. G. Riess et al. 2022), a log-normal distribution for $\zeta_e \gamma_{\mathrm{th}}^2 (R/0.01\ \mathrm{pc})^2$ with ($\mu = 0$, $\sigma = 0.5$), and a uniform prior for $\mathrm{DM_{host}} + \mathrm{DM_{src}}$ within $(0, 1500)\,\mathrm{pc\,cm^{-3}}$. Results are shown in Figure 2.
4. *Second-stage MCMC*. The posterior distribution of $\zeta_e \gamma_{\mathrm{th}}^2 (R/0.01\quad \mathrm{pc})^2$ from the first stage is used as a prior to fit Equation (2). A uniform prior for H_0 is adopted within (0, 140). Results are shown in Figure 3. The final posterior

[5] A conversion from event-rate density to redshift rate distribution is needed (e.g., R. C. Zhang et al. 2021).

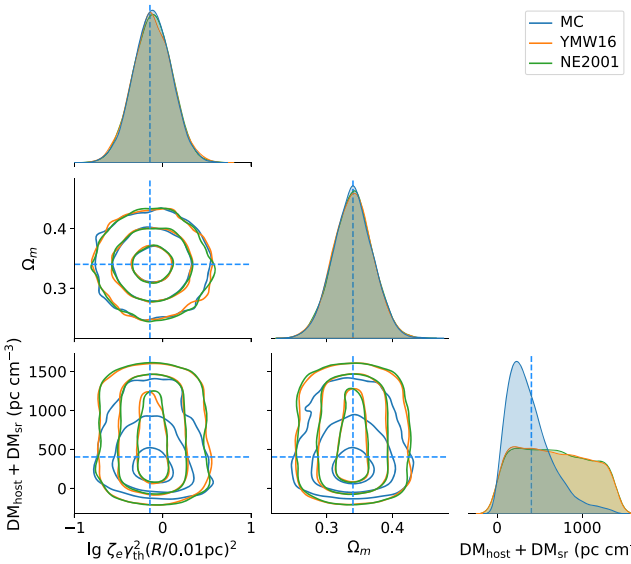

Figure 2. Posterior distributions from MCMC analyses of Equation (6). The contour plot is smoothed using kernel density estimation. Blue, orange, and green solid lines correspond to fitting results for detected mock PRSs and real PRSs analyzed using the YMW16 model and the NE2001 model, respectively. In each contour set, 1σ, 2σ, and 3σ confidence regions appear from innermost to outermost. Blue dashed lines indicate the median values of the injected distributions of the Monte Carlo simulation.

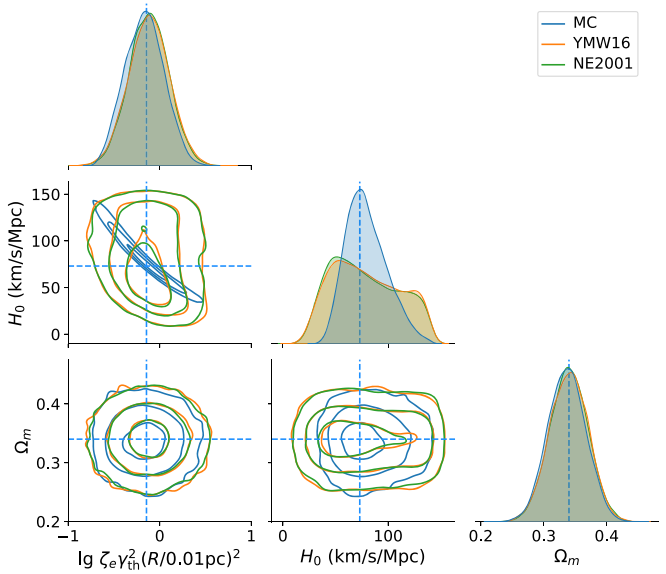

Figure 3. Posterior distributions from MCMC analyses of Equation (2). The posterior distribution of lg $\zeta_e\gamma_{\rm th}^2(R/0.01$ pc$)^2$ in Figure 2 is adopted as the prior distribution.

distribution of $\zeta_e\gamma_{\rm th}^2(R/0.01$ pc$)^2 \sim 1$ is expected as the first glance at luminosity–RM relation (G. Bruni et al. 2025). We get $H_0 = 75 \pm 30\,{\rm km\,s^{-1}\,Mpc^{-1}}$ for observed PRSs by YMW16 and NE2001 models, which shows our method is insensitive to the Galactic electron number density models. For the mock sample, we get $H_0 = 75 \pm 15\,{\rm km\,s^{-1}\,Mpc^{-1}}$, consistent with our injection assumption.

4. Summary and Discussion

1. Traditional FRB cosmology struggles with overlapping dependencies among H_0, Ω_b, and $f_{\rm IGM}$. The Yang relation (Y.-P. Yang et al. 2020) can help to disengage this by incorporating RM to link PRS luminosity to the magneto-ionic environment of FRBs, alleviating degeneracies inherent in DM-only methods.
2. The principal aim of this study is to demonstrate the feasibility of using the Yang relation to constrain cosmological parameters. We begin by generating a mock PRS sample. As a secondary investigation, we perform a preliminary population study of PRSs. We find that the redshift distribution follows cosmic star formation, the luminosity function follows a power law ($\Phi(L_\nu) \propto L_\nu^{-1.3}$), and the parameter $\zeta_e\gamma_{\rm th}^2(R/0.01$ pc$)^2$ follows a log-normal distribution ($\mu = -0.333$, $\sigma = 0.6$), in line with current observational data.
3. We introduce a two-stage MCMC framework to constrain H_0. First, we derive the product $\zeta_e\gamma_{\rm th}^2(R/0.01$ pc$)^2$ using DM observations (Equation (6)), then use the result as priors to estimate H_0 (Equation (2)). For our mock sample, this procedure yields $H_0 = 75 \pm 15\,{\rm km\,s^{-1}\,Mpc^{-1}}$, consistent with the injected value. Applying the method to six observed PRSs gives $H_0 = 75 \pm 30\,{\rm km\,s^{-1}\,Mpc^{-1}}$ for both the YMW16 and NE2001 models, indicating insensitivity to specific Galactic density models.
4. However, a degeneracy remains between $\zeta_e\gamma_{\rm th}^2R^2$ and H_0 (Figure 3), highlighting the need for further refinements. Future advancements will benefit from a larger PRS sample enabled by interferometric facilities (e.g., CHIME Outrigger, A. E. Lanman et al. 2024; MeerKAT, J. Jonas & MeerKAT Team 2016; ASKAP, A. W. Hotan et al. 2021; Very Large Array, VLA, R. A. Perley et al. 2011; DSA-2000, G. Hallinan et al. 2024; and Square Kilometre Array, P. E. Dewdney et al. 2009), which improve the statistics. With a bigger sample, a full Bayesian treatment, incorporating carefully considered prior distributions of all parameters (e.g., different DM components, $f_{\rm IGM}$, Ω_b), can refine constraints on cosmological parameters (e.g., J. P. Macquart et al. 2020; Q. Wu et al. 2022).
5. Improved constraints on $\zeta_e\gamma_{\rm th}^2R^2$ may be obtained through observation and theoretical modeling. Observationally, high-resolution radio imaging and multiwavelength observations can constraint the physical size R of the nebula and thereby limit $\zeta_e\gamma_{\rm th}$. For example, recent observations of the hyperactive FRB 20240114A show an evolving absorption frequency in its PRS (X. Zhang et al. 2025), which could be related to $\gamma_{\rm th}$. Theoretically, modeling PRSs within frameworks such as supernova remnant or magnetar wind nebula models can further clarify their evolutionary patterns.
6. A promising strategy for using the Yang relation is to calibrate $\zeta_e\gamma_{\rm th}^2R^2$ by observing another standard candle in the same host galaxy, akin to the approach of calibrating absolute magnitudes for Type Ia supernovae (e.g., C. T. Kowal 1968; D. Branch & G. A. Tammann 1992). This approach avoids uncertainties and degeneracies inherent to pure DM methods. The persistent nature of PRSs enables repeated host galaxy observations targeting Type Ia supernovae, which provide independent constraints on $\zeta_e\gamma_{\rm th}^2R^2$. Assuming the luminosity of FRB 20190520B's PRS, we estimate the detectability of PRSs out to $z \sim 0.8$, which demonstrates PRSs as viable cosmological probes.

7. In principle, this strategy can be applied to any PRS exhibiting analogous characteristics, regardless of whether it is associated with an FRB. Y. Dong et al. (2024) have identified continuous compact radio sources with VLA that are not linked to FRBs but may represent older PRSs; if these sources share the same emission mechanism as those associated with FRBs and have RM measured,[6] they could similarly be used to constrain cosmological parameters using the Yang relation.

Acknowledgments

Z.Z. recalls that this idea first came to his mind when his thoughts drifted off during an astrophysics class. Z.Z. thanks Hua Chen and Jia-Ming Zhu-Ge for helpful discussions. We thank the referee for helpful comments. This work is supported by the Nevada Center for Astrophysics, a TTDGRA fellowship at UNLV, and NASA 80NSSC23M0104.

Software: astropy (Astropy Collaboration et al. 2022), NumPy (C. R. Harris et al. 2020), Matplotlib (J. D. Hunter 2007), emcee (D. Foreman-Mackey et al. 2013), SciPy (P. Virtanen et al. 2020), seaborn (M. L. Waskom 2021).

ORCID iDs

Zi-Liang Zhang (张子良) https://orcid.org/0000-0002-9110-4336
Bing Zhang (张冰) https://orcid.org/0000-0002-9725-2524

References

Anna-Thomas, R., Connor, L., Dai, S., et al. 2023, Sci, 380, 599
Astropy Collaboration, Price-Whelan, A. M., Lim, P. L., et al. 2022, ApJ, 935, 167
Bassa, C. G., Tendulkar, S. P., Adams, E. A. K., et al. 2017, ApJL, 843, L8
Beniamini, P., Kumar, P., Ma, X., & Quataert, E. 2021, MNRAS, 502, 5134
Bernales-Cortes, L., Tejos, N., Prochaska, J. X., et al. 2025, arXiv:2501.14063
Bhandari, S., & Flynn, C. 2021, Univ, 7, 85
Bhusare, Y., Maan, Y., & Kumar, A. 2024, ATel, 16820, 1
Branch, D., & Tammann, G. A. 1992, ARA&A, 30, 359
Bruni, G., Piro, L., Yang, Y.-P., et al. 2024, Natur, 632, 1014
Bruni, G., Piro, L., Yang, Y. P., et al. 2025, A&A, 695, L12
Caleb, M., Flynn, C., & Stappers, B. W. 2019, MNRAS, 485, 2281
Chatterjee, S., Law, C. J., Wharton, R. S., et al. 2017, Natur, 541, 58
Chen, X.-L., Tsai, C.-W., Li, D., et al. 2025, ApJL, 980, L24
Chittidi, J. S., Simha, S., Mannings, A., et al. 2021, ApJ, 922, 173
Cooke, R. J., Pettini, M., & Steidel, C. C. 2018, ApJ, 855, 102
Cordes, J. M., & Chatterjee, S. 2019, ARA&A, 57, 417
Cordes, J. M., & Lazio, T. J. W. 2002, arXiv:astro-ph/0207156
Dai, Z. G., Wang, J. S., & Yu, Y. W. 2017, ApJL, 838, L7
Deng, W., & Zhang, B. 2014, ApJL, 783, L35
Dewdney, P. E., Hall, P. J., Schilizzi, R. T., & Lazio, T. J. L. W. 2009, IEEEP, 97, 1482
Dong, Y., Eftekhari, T., Fong, W., et al. 2024, ApJ, 973, 133
Foreman-Mackey, D., Hogg, D. W., Lang, D., & Goodman, J. 2013, PASP, 125, 306
Fukugita, M., Hogan, C. J., & Peebles, P. J. E. 1998, ApJ, 503, 518
Gao, H., Li, Z., & Zhang, B. 2014, ApJ, 788, 189
Glowacki, M., & Lee, K.-G. 2024, arXiv:2410.24072
Gupta, O., Beniamini, P., Kumar, P., & Finkelstein, S. L. 2025, arXiv:2501.09810
Hallinan, G., Ravi, V., Bouman, K., et al. 2024, AAS Meeting Abstracts, 243, 237.05
Harris, C. R., Millman, K. J., van der Walt, S. J., et al. 2020, Natur, 585, 357
Hotan, A. W., Bunton, J. D., Chippendale, A. P., et al. 2021, PASA, 38, e009
Hunter, J. D. 2007, CSE, 9, 90
Ibik, A. L., Drout, M. R., Gaensler, B. M., et al. 2024, ApJ, 976, 199
James, C. W., Ghosh, E. M., Prochaska, J. X., et al. 2022b, MNRAS, 516, 4862
James, C. W., Prochaska, J. X., Macquart, J. P., et al. 2022a, MNRAS, 510, L18
Jonas, J. & MeerKAT Team 2016, in Proc. of MeerKAT Science: On the Pathway to the SKA (Trieste: PoS)
Kokubo, M., Mitsuda, K., Sugai, H., et al. 2017, ApJ, 844, 95
Kovacs, T. O., Mao, S. A., Basu, A., et al. 2024, A&A, 690, A47
Kowal, C. T. 1968, AJ, 73, 1021
Lanman, A. E., Andrew, S., Lazda, M., et al. 2024, AJ, 168, 87
Li, Q.-C., Yang, Y.-P., & Dai, Z.-G. 2020a, ApJ, 896, 71
Li, Y., & Zhang, B. 2020, ApJL, 899, L6
Li, Y., Zhang, B., Nagamine, K., & Shi, J. 2019, ApJL, 884, L26
Li, Z., Gao, H., Wei, J. J., et al. 2020b, MNRAS, 496, L28
Lorimer, D. R., Bailes, M., McLaughlin, M. A., Narkevic, D. J., & Crawford, F. 2007, Sci, 318, 777
Macquart, J. P., Prochaska, J. X., McQuinn, M., et al. 2020, Natur, 581, 391
Madau, P., & Dickinson, M. 2014, ARA&A, 52, 415
Manchester, R. N., Hobbs, G. B., Teoh, A., & Hobbs, M. 2005, AJ, 129, 1993
Margalit, B., Berger, E., & Metzger, B. D. 2019, ApJ, 886, 110
Margalit, B., & Metzger, B. D. 2018, ApJL, 868, L4
Margalit, B., Metzger, B. D., Berger, E., et al. 2018, MNRAS, 481, 2407
McQuinn, M. 2014, ApJL, 780, L33
Metzger, B. D., Berger, E., & Margalit, B. 2017, ApJ, 841, 14
Michilli, D., Seymour, A., Hessels, J. W. T., et al. 2018, Natur, 553, 182
Mo, J.-F., Zhu, W., Wang, Y., Tang, L., & Feng, L.-L. 2023, MNRAS, 518 539
Murase, K., Kashiyama, K., & Mészáros, P. 2016, MNRAS, 461, 1498
Niu, C. H., Aggarwal, K., Li, D., et al. 2022, Natur, 606, 873
Orr, M. E., Burkhart, B., Lu, W., Ponnada, S. B., & Hummels, C. B. 2024, ApJL, 972, L26
Perley, R. A., Chandler, C. J., Butler, B. J., & Wrobel, J. M. 2011, ApJL, 739, L1
Petroff, E., Hessels, J. W. T., & Lorimer, D. R. 2022, A&ARv, 30, 2
Piro, L., Bruni, G., Troja, E., et al. 2021, A&A, 656, L15
Planck Collaboration, Aghanim, N., Akrami, Y., et al. 2020, A&A, 641, A6
Prochaska, J. X., & Zheng, Y. 2019, MNRAS, 485, 648
Quataert, E., & Gruzinov, A. 2000, ApJ, 545, 842
Ravi, V., Law, C. J., Li, D., et al. 2022, MNRAS, 513, 982
Riess, A. G., Yuan, W., Macri, L. M., et al. 2022, ApJL, 934, L7
Reissl, S., Klessen, R. S., Pellegrini, E. W., et al. 2023, NatAs, 7, 1295
Shin, K., Masui, K. W., Bhardwaj, M., et al. 2023, ApJ, 944, 105
Sridhar, N., & Metzger, B. D. 2022, ApJ, 937, 5
Tendulkar, S. P., Bassa, C. G., Cordes, J. M., et al. 2017, ApJL, 834, L7
Theis, A., Hagstotz, S., Reischke, R., & Weller, J. 2024, arXiv:2403.08611
Thornton, D., Stappers, B., Bailes, M., et al. 2013, Sci, 341, 53
Virtanen, P., Gommers, R., Oliphant, T. E., et al. 2020, NatMe, 17, 261
Wang, Y., & van Leeuwen, J. 2024, A&A, 690, A377
Wang, Y.-Y., Gao, S.-J., & Fan, Y.-Z. 2025, ApJ, 981, 9
Waskom, M. L. 2021, JOSS, 6, 3021
Wu, Q., & Wang, F.-Y. 2024, ChPhL, 41, 119801
Wu, Q., Zhang, G.-Q., & Wang, F.-Y. 2022, MNRAS, 515, L1
Xu, H., Niu, J. R., Chen, P., et al. 2022, Natur, 609, 685
Yang, Y.-P., Lu, W., Feng, Y., Zhang, B., & Li, D. 2022, ApJL, 928, L16
Yang, Y.-P., Li, Q.-C., & Zhang, B. 2020, ApJ, 895, 7
Yang, Y.-P., Luo, R., Li, Z., & Zhang, B. 2017, ApJL, 839, L25
Yang, Y.-P., Zhang, B., & Dai, Z.-G. 2016, ApJL, 819, L12
Yao, J. M., Manchester, R. N., & Wang, N. 2017, ApJ, 835, 29
Zhang, B. 2023, RvMP, 95, 035005
Zhang, G. Q., Yu, H., He, J. H., & Wang, F. Y. 2020, ApJ, 900, 170
Zhang, R. C., & Zhang, B. 2022, ApJL, 924, L14
Zhang, R. C., Zhang, B., Li, Y., & Lorimer, D. R. 2021, MNRAS, 501, 157
Zhang, X., Yu, W., Yan, Z., Xing, Y., & Zhang, B. 2025, arXiv:2501.14247
Zhang, Z. J., Nagamine, K., Oku, Y., et al. 2025, arXiv:2503.12741
Zhang, Z.-L., Yu, Y.-W., & Cao, X.-F. 2023, A&A, 675, A66
Zhao, Z. Y., & Wang, F. Y. 2021, ApJL, 923, L17
Zheng, Z., Ofek, E. O., Kulkarni, S. R., Neill, J. D., & Juric, M. 2014, ApJ, 797, 71
Zhou, B., Li, X., Wang, T., Fan, Y.-Z., & Wei, D.-M. 2014, PhRvD, 89, 107303

[6] Notice that the RM of FRBs can be measured from its bright polarized pulses; it remains uncertain whether the continuous emission from PRSs is sufficiently polarized to allow a robust RM measurement.